photonics

MDPI

Article

Space–Time Wavepackets from the Perspective of Needle Beams

Ruediger Grunwald * and Martin Bock

Max-Born-Institute for Nonlinear Optics and Short Pulse Spectroscopy, Max-Born-Strasse 2a, 12489 Berlin, Germany; mbock@mbi-berlin.de
* Correspondence: grunwald@mbi-berlin.de

Abstract

The propagation of coherent quasi-nondiffracting (QND) space–time wavepackets (STWPs) is studied by numerical simulations. The concept of "elementary needle beams" (NBs) as building blocks for structured wavepackets is presented, which exploits specific advantages like spectral invariance, simplicity of generation and robustness. Two different approaches for shaping STWPs are compared to each other with respect to their spectral propagation characteristics. The results indicate that, in defined parameter windows, Bessel–Gauss needle beam type STWPs (BG-NB) can reach higher spectral and temporal homogeneity and bandwidth tolerance compared to spatio-spectrally pre-shaped Gaussian foci (PS-GF). Simulations for arrays of femtosecond NBs show, in agreement with previous experiments, a periodical field replication in space and time with low pulse distortion. Unlike the classical diffractive Talbot effect, nondiffracting self-imaging enables operation with large spectral bandwidth and ultrashort pulse durations, thus promising advanced applications in optical processing and sensing. Further topics in the research area are addressed in a brief overview.

Keywords: space–time wavepackets; nondiffracting needle beams; beam propagation; nondiffracting Talbot effect; spatio-spectral shaping; ultrashort pulses; spectral homogeneity; bandwidth tolerance; arrays of wavepackets; space–time wavepackets with orbital angular momentum

1. Introduction

Strong localization and structuring of light in space and time is of exceptional interest for an improved understanding of light–matter interactions as well as for modern quantum technologies [1,2]. Certain types of localized beams exhibit needle-like propagations zones, making them attractive for applications that require a high concentration of photons and/or high resolution. Other important aspects are related to their propagation stability.

Recently, we gave an overview on different classes of "needle beams" (NBs) with particular emphasis on quasi-nondiffracting (QND) propagation [3]. Such beams offer an alternative to other optical STWPs based on spatio-spectral management [4,5], which are currently the subject of intense research [6–9]. NBs are described by propagation-invariant solutions to the wave equation [10] under specific boundary conditions. Bessel-like beams are typically generated by phase shaping axicons. To filter out central Bessel lobes at minimal diffraction, self-apodized truncation has proved to be an optimum approach [11–13]. At small angles, which can be realized by thin-film optics or spatial light modulators (SLMs), extended zones of undistorted propagation are generated [14]. By truncating Bessel beams at higher order minima, even a further reduction in divergence is feasible [15]. Other advantageous properties of NBs are self-healing [1] and spectral–temporal robustness [16].

Check for updates

Received: 9 October 2026
Revised: 12 November 2026
Accepted: 16 November 2026
Published: 19 November 2026

Copyright: © 2026 by the authors. Licensee MDPI, Basel, Switzerland. This article is an open access article distributed under the terms and conditions of the Creative Commons Attribution (CC BY) license.

Therefore, the necessity of an extension of the NB approach to ultrashort-pulsed and complex structured beams including highly localized wavepackets [17–19] is obvious.

Here, we discuss the concept of synthesizing structured STWPs by combining "elementary needle beams". The basic idea is illustrated through the example of a single-coil "optical spring". Spatio-spectral and spatio-temporal properties of selected types of QND-STWPs (BG-NB and PS-GF) are studied by numerical simulations. Particular emphasis is laid on the comparison of their spectral homogeneity and bandwidth transfer. The impact of geometrical conditions like spatial frequency filtering apertures is addressed.

In further simulations, multiple NBs are combined to structured STWPs which are shaped as hexagonal arrays of NBs. The phenomenon of nondiffracting self-imaging of NBs [20] is examined for such arrays with and without non-zero topological charge. The findings on the extraordinary temporal transfer are discussed in detail and possible applications are suggested.

Finally, current topical issues and trends in the field of research are briefly addressed.

2. Concept of Space–Time Wavepackets as Compositions of Elementary Needle Beams

In temporal and spectral domains, quasi-nondiffracting conditions are of fundamental importance, as they allow for stable pulse duration and conserved spectral bandwidth throughout the entire zone of invariant propagation. In the course of the development of acoustics and electromagnetics, non-spreading wavepackets were approximated in two different ways. On the one hand, stable solutions of wave equations were identified by theory (compare ref. [1]) (bottom-up approach). On the other hand, complex STWPs were synthesized by transforming or combining pulsed Gaussian laser beams while following inverse design strategies (top-down approach). In this framework, the geometric-optical concept of caustics has proven to be a useful approach [21]. At ultrashort pulse durations, the classical picture of beams has to be replaced by propagation traces of traveling wavepackets. For tailoring structured STWPs, space–time coupling, including the complete angular-dependent pulse travel time, dispersion and diffraction effects, has to be taken into account [22–31]. The theoretical treatment of structured STWPs is anything but trivial because of specific constraints concerning the simultaneous control of temporal and 3D spatial parameters. Closed-form expressions with spherical wavefronts were published for rotationally symmetric needle pulses [32]. Spatially dependent frequency control is used to compensate propagation dependent frequency shifts. The complex dynamics of ultrashort-pulsed light fields requires searching for simple and experimentally accessible approaches for inverse design strategies [33]. A particular inverse design based on a stationary phase approximation was proposed that provides arbitrary trajectories under non-paraxial conditions. In analogy to the angular spectrum representation of free-space optical modes, elementary needle-shaped wavepackets can be used to decompose or to construct complex spatio-temporal structures. By proof-of-principle experiments, the composition of structured STWPs by "elementary" NBs was shown to be a simple but promising approach [17–19]. The technical approximation can be realized by phase-front shaping with two-dimensional arrays of refractive, reflective or diffractive micro-axicons. Balancing diffractive and refractive parameters allows to efficiently minimize dispersion [22]. Flexible shaping of structured STWPs with tunable axicons or spiral phase plates was demonstrated by applying liquid-crystal SLMs [17–19] and actuated micro-mirrors [34–36]. Digital mirrors have also been proven to be suitable components for dynamically adjusting the required spectral phase in stretcher–compressor systems [37]. Related techniques enable pulse shaping through dispersion control. Purely reflective SLMs are suitable for

transforming few-cycle pulses, however, in practice, they are subject to certain limitations regarding spatial resolution, the number of sub-apertures, phase range, and lifetime.

Figure 1a–d illustrate the principle of synthesizing few-cycle STWPs by combining "elementary needle beams" through the example of an optical vortex. To approximate a single-coil ("optical spring"), a discretized theoretical model was applied for design and optimization. To approximate the target structure, N axicon-generated NBs have to be arranged along a circle of radius R_0 with a step-by-step increasing phase. The spatial- and time-dependent electrical field of the beam array can be written in the form

$$E(r,\ t) = \sum_{n=0}^{N-1} A_n \cdot exp\left(-\frac{\left((x-x_n)^2+(y-y_n)^2\right)}{w_0^2}\right) \cdot exp\left(-\frac{(t-t_n)^2}{2\tau^2}\right) \cdot cos[\omega_0(t-t_n) - l\theta_n] \quad (1)$$

where $(x_n, y_n) = (R_0 \cos\theta_n, R_0 \sin\theta_n)$ define the coordinates of the beam centers for azimuthal angles $\theta_n = 2\pi j/N$, $\boldsymbol{\tau}$ and l the topological charge and the pulse duration, and t_n represents the individual temporal delay imparted to the j-th needle beam by the initial phases:

$$t_n = \frac{\theta_n}{2\pi} \cdot T_{coil} \quad (2)$$

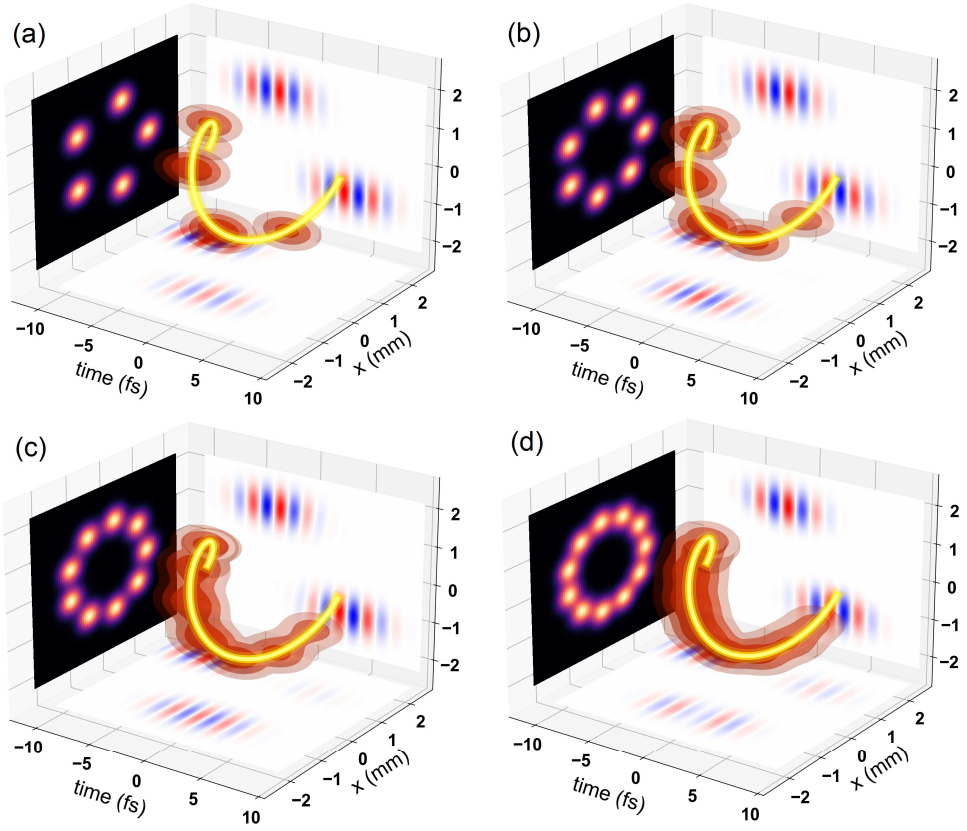


Figure 1. Principle of composing structured STWPs by elementary NBs. The example shows the generation of a space–time vortex (single-coil "optical spring") by controlling phase and tilt of multiple few-cycle pulsed NBs (schematically). The number of elementary NBs in (**a**–**d**) varies from 5 to 11 to visualize the approximation of a continuous STWP envelope by discrete building blocks (black plane: intensity disdribution; space-time projections: positive (red) and negative (blue) field amplitudes; orange curve: 3D field isosurface with yellow guide line) The basic approach simplifies the design of complex STWPs and facilitates the interpretation of certain propagation phenomena.

Thus, a complete rotation around the central singularity corresponds to a phase step of $2\boldsymbol{\pi}$ and a maximum travel time difference in T_{coil}.

A major advantage of the SLM-based architecture is the complete decoupling of the ring geometry from the topological charge l. In standard Laguerre–Gaussian or Bessel vortices, the dark-core radius strictly scales with l ($R_{ring} \propto |l|$). In our approach based on using elementary NBs as building blocks for structured STWPs, the ring radius R_{ring} is specified independently by the programmed needle locations, while a subsequent 2π-spiral phase profile imparts an OAM without expanding the transverse beam diameter.

In reverse order, a multichannel nonlinear autocorrelation was used on the detection side to spatially separate nondiffracting components of a fs-vortex (corresponding to "elementary needle beams") and to extract the phase envelope by analyzing the azimuthally dependent shift in the local (virtual) "beamlets". Corresponding experimental results were published elsewhere [38].

The optimization of structured STWPs on the basis of the described concept requires a detailed analysis of the propagation and interference properties of NBs, which goes beyond the current state of mostly empirical experimental approaches with few-cycle pulses. Therefore, corresponding numerical simulations of the propagation of wavepackets on an ultrafast time-scale were performed for two relevant sub-problems of the concept of elementary NBs, the spectral fine structure of NBs and the self-imaging of arrays of NBs in space and time.

3. Theoretical Models and Computational Methods

Needle-shaped STWPs can be generated by transforming ultrashort-pulsed, broadband Gaussian laser beams by different optical techniques. We compare two particular approaches with each other in wave propagation simulations with Python 3.9.13 software.

Method I uses the spatial transformation of a pulsed beam with axicons into a Bessel–Gaussian needle beam (BG-NB). The alternative *Method II* generates a comparably extended QND zone through the spectral pre-shaping of a Gaussian focus (PS-GF). This so-called "light-cone intersection approach" was studied extensively by the group of Ayman F. Abouraddy at CREOL [7,39,40]. The advantage of a spectral management of a Gaussian focus consists of enabling, in some limits with respect to the bandwidth, to compensate for pulse broadening by dispersion. The parameters for the numerical simulation of the BG-NB were chosen to be compatible with realistic experimental conditions and largely align with the data reported in the literature [39] or PS-GF-that is, concentrating a comparable amount of energy within a comparable geometric region.

The propagation was simulated for a complex electric field $E(x, y, z, t)$ in a 3D spatio-temporal grid (x, y, t). This framework allows a direct comparison between the selected methods. The initial scalar field at the input plane $(z = 0)$ for both configurations is defined by combining a zero-order Bessel function yielding a transverse needle beam profile with a Gaussian spatial amplitude envelope:

$$E(\mathrm{x},\ \mathrm{y}, 0, \omega)\ = J_0\left(\mathrm{k}_\perp \sqrt{x^2\ +\ y^2}\right) \exp\left(-\frac{x^2 + y^2}{w_0^2}\right) \mathrm{S}(\mathrm{x}, \omega) \tag{3}$$

where $k_\perp = k_0 \sin\theta$ denotes the transverse wave vector corresponding to a propagation angle θ, $S(x, \omega)$ describes the spatio-spectral distribution, and w_0 represents the beam waist radius. For the reference NB, the wavelength remains uniform across the beam profile $(\lambda = \lambda_0)$. In contrast, the implementation of the STWP from *Method II*, mimicking a 4f-SLM pulse shaper configuration introduces a deterministic correlation between the local transverse spatial frequencies (k_x) and effective central wavelengths $\lambda_{eff}(k_x)$. This parabolic coupling relation is given by:

$$\lambda_{eff}(\mathrm{k}_x)\ = \lambda_0\ -\ \Delta\lambda_{max}\left(-\frac{k_x}{k_{x,max}}\right) \tag{4}$$

where λ_0 is the central wavelength and $\Delta\lambda_{\max}$ represents the maximum spectral shift tolerated by the system's aperture and angular dispersion limits. To evaluate the propagation along the longitudinal coordinate z, the initial field is transformed into the spatial frequency and spectral domain via 3D Fourier transform:

$$\tilde{\mathrm{E}}\left(k_x,\ k_y,\ 0,\omega\right)\ = \mathcal{F}\{\mathrm{E}(x,y,0,t)\} \tag{5}$$

The propagation over a distance z is then calculated rigorously using the exact transfer function:

$$\tilde{\mathrm{E}}\left(k_x,\ k_y,\ z,\omega\right)\ = \tilde{\mathrm{E}}\left(k_x,\ k_y,\ 0,\omega\right)\exp\left[i\mathrm{k}_z\left(k_x,k_y,\omega\right)z\right] \tag{6}$$

where the longitudinal wave vector component k_z satisfies the dispersion relation:

$$k_z(k_x,k_x,\omega) = \sqrt{\left(\frac{\omega}{c}\right)^2 - {k_x}^2 - {k_z}^2} \tag{7}$$

The fully resolved spatio-temporal field $E(x, y, z, t)$ in the real-space and time domain is recovered via inverse Fourier transformation:

$$E(x,y,z,t)\ = \mathcal{F}^{-1}_{k_x,k_y,\omega}\left\{\tilde{E}\left(k_x,\ k_y,\ z,\omega\right)\right\} \tag{8}$$

To account for finite aperture constraints and non-paraxial propagation effects in realistic experimental realizations, an empirical axial envelope function $A(z)$ is incorporated to modulate the longitudinal intensity decay. The resulting output intensity distributions $I(x, z) = |E(x,z)|^2$ are normalized to the peak intensity to highlight the distinct propagation invariants of the needle beam versus the coupled STWP dynamics. Furthermore, bandwidth limitations governed by aperture filtering in the Fourier plane are modeled via an exponential saturation function:

$$\Delta\lambda_{out} = 2\Delta\lambda_{max}\left[1 - exp\left(-\frac{\Delta\lambda_{in}}{\Delta\lambda_{max}}\right)\right] \tag{9}$$

The transverse spectral homogeneity σ_λ, i.e., the spatial standard deviation of the effective wavelength across the beam cross-section, is defined as follows:

$$\sigma_\lambda = \sqrt{\left\langle\left(\lambda_{eff}(x) - \lambda_0\right)^2\right\rangle} \tag{10}$$

The propagation of the femtosecond needle beam array with and without topological charge were investigated using a rigorous numerical model based on scalar diffraction theory and angular spectrum propagation in the frequency domain.

The initial electric field envelope at the plane $z = 0$ is modeled as a product of a fundamental Gaussian beam profile $E_0(x,y)$ and a complex transmission function representing the hexagonal axicon array:

$$E(x,y,\omega_0) = E(x,y)\sum_n exp[(i(\Phi_{axicon}(r_n) + \ell\cdot\varphi_n)]apod(r_n) \tag{11}$$

For each individual axicon centered at (cx_n,cy_n), local polar coordinates (r_n,φ_n) are defined. The phase mask combines the conical axicon phase $\Phi_{\mathrm{axicon}}(r_n) = -k_0(n_{\mathrm{axicon}} - 1)\alpha$ $r_n + \pi$ with a spiral phase $\ell\varphi_{\mathrm{n}}$ corresponding to an integer topological charge ℓ. A high-order super-Gaussian aperture function $apod = \exp\ (-[r_n/R]^{\mathrm{N}})$ is applied to each element to eliminate high-frequency edge-diffraction artifacts. In our calculations, an appropriately high N was chosen adaptively. To account for spatial–temporal coupling and pulse front deformations associated with ultrashort pulses (τ_{p} = 20 fs FWHM), the optical field is decomposed into $N_\lambda = 256$ discrete spectral components spanning the broadband spectrum

around λ_0. Each spectral component is assigned a Gaussian weighting corresponding to the transform limited pulse duration.

The 2D spatial Fourier transform of the initial field is propagated along the longitudinal axis z using the exact angular spectrum transfer function:

$$H\left(f_x, f_y, z, \lambda\right) = \exp\left(iz\sqrt{\left[k^2 - 4\pi^2\left(f_x{}^2 + f_y{}^2\right)\right]}\right) \quad (12)$$

The global 3D intensity distribution $I(x, y, z)$ is obtained by inverse Fourier transformation back to the spatial domain for each monochromatic component and subsequent incoherent integration across time. To resolve local spatial–temporal pulse profiles $I(x,t)$ or $I(y,t)$ at planes of interest, a moving temporal frame (retarded time $t_{ret} = t - z/c$) combined with carrier-envelope demodulation $(\omega - \omega_0)$ is implemented. This accurately captures subluminal group velocity dynamics and optical path variations. The simulations were performed on a high-resolution Cartesian grid ($N_x \cdot N_y = 256 \cdot 256$ pixels). The spectral resolution was chosen to be about $\Delta\lambda = 1$ nm, and the total temporal window comprised 400 steps of 1 fs for each set of calculations. Computational efficiency was achieved by implementing a parallelized processing pipeline along the longitudinal propagation coordinates (z-planes) utilizing Python's *joblib* framework.

4. Results of Numerical Simulations

4.1. Propagation of Needle-like STWPs Generated by Spatial and Spatio-Spectral Shaping

The numerically simulated intensity and spectral propagation characteristics of the two selected types of needle-like STWPs are compared with each other in Figure 2. The images on top and button show the calculated propagation zones according to *Method I* and *Method II*, respectively. Both intensity propagation plots in Figure 2a,b show needle-shaped geometries. The spectral propagation characteristics indicate a higher radial homogeneity of the spectral content for the BG-NBs (Figure 2c) compared to the spectrally confined Gaussian focus PS-GF (Figure 2d).

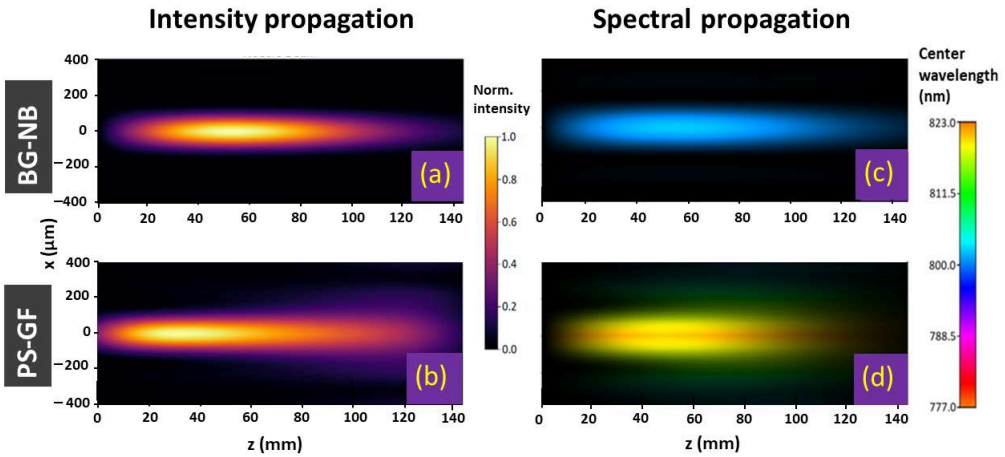


Figure 2. Simulated propagation of two types of needle-shaped STWPs in spatial and spectral domain: (**a**,**c**) Bessel–Gauss needle beams (BG-NBs) (color code: relative intensity), (**b**,**d**) pre-shaped Gaussian focus (PS-GF) (color code: center wavelength). PS-GF simulations were carried out with spatio-spectral shaping according to ref. [39]. The parameters for BG-NB were matched to enable a direct comparison (axicon illuminated by a Gaussian-shaped laser beam, central wavelength 800 nm, pulse duration 20 fs, axicon angle 0.1°, refractive index 1.45, initial beam diameter 500 µm).

For both cases, the numerical simulations provide needle-like propagation zones of relatively similar geometry. This is less surprising because both approaches are based

on reshaping Gaussian beams (spatially by *Method I*, spatio-spectrally by *Method II*). One observes an axial shift in the intensity maxima and varying beam shapes. With longer distances, larger beam diameters show up for the PS-GF whereas a more distinct needle geometry is found for the BG-NB. The spectral distribution of both types of STWPs is not identical. In particular, a significant radial inhomogeneity appears for PS-GF. The corresponding physics will have to be discussed later in more detail (see Section 5.1).

4.2. Spatio-Temporal Self-Imaging of Arrays of Ultrashort-Pulsed NBs

4.2.1. Propagation of Arrays of Needle Beams (NB-A)

If structured STWPs are composed of ultrashort-pulsed, coherent elementary NBs, the mutual phase relationships play a decisive role. The interference of spatially periodic arrangements of pulsed NBs gives rise to a specific self-imaging behavior (also referred to as "nondiffracting Talbot effect" or "geometrical Talbot effect") where the field structure does not depend on the wavelength and experiences a quasi-periodic revival of arrays both in space and time [3,20,41,42]. In our simulations, we calculated corresponding space–time propagation patterns for two different types of hexagonal STWP arrays under coherent pulsed Bessel–Gauss beam illumination. Conical angular spectra without and with additional phase vortices were generated by hexagonal arrangements of virtual (i) axicons and (ii) spiral phase plates (SPPs). All parameters were chosen to simulate typical experimental conditions with a central laser wavelength of $\lambda = 800$ nm, a pulse duration of $\tau = 20$ fs, axicon angle of $\alpha = 0.24°$, a hexagonal array geometry with a period of $p = 400$ µm, an axicon refractive index of $n = 1.45$, and an illuminating Gaussian beam diameter of $2w_0 = 5$ mm. In the following, both related array configurations (NB-A) and (OAM-A) are compared with respect to their propagation characteristics in space and time. The propagation of ultrashort-pulsed NB arrays (NB-A) with a topological charge $l = 0$ was simulated on the basis of the parameters listed in the previous sub-section. The spatial and temporal self-imaging properties will be presented separately to better visualize the specific features and to match potential applications and characterization techniques. The two-dimensional phase mask of a hexagonal axicon array is plotted in Figure 3a. Axial cuts of the intensity distribution (Figure 3b,c) and transversal intensity carpets for focal distance, first out-of-phase and two in-phase Talbot distances (Figure 3d–g) characterize the propagation from orthogonal perspectives. Neglecting diffraction, the purely geometrical theory predicts the appearance of nondiffracting Talbot planes at discrete distances [20]

$$L_{nd} = N\frac{a}{tan\theta} + \frac{ad}{4\ tan\theta} \tag{13}$$

(a = array period, d = axicon diameter, θ = half conical beam angle, and $N = 1, 2, 3...$ are integer numbers denoting subsequent nondiffracting Talbot planes).

Periods $> a$ are not considered in Equation (13) but are expected to cause some parasitic interferences in experiments (interference of shaped and unshaped parts). The dissipation of light out of the overlapping zone by divergence and space–time coupling lead, in agreement with experimental results, to decreasing peak intensities towards larger N and a significantly limited number of Talbot planes. The applied parameters including a pulse duration of $\boldsymbol{\tau} = 20$ fs (about seven cycles of the optical field) enable the generation of some three nondiffracting Talbot planes of high contrast at distances of up to >60 cm.

The temporal structure of the array is depicted in Figure 4a,b for five sub-beams (radial cut in x-direction at $y = 0$). The oscillating intensity of a selected peak in Figure 4c (central cut) clearly indicates the self-imaging of the STWP array in the time domain and enables to predict, for the chirp-free case, the change in the pulse duration by spatio-temporal coupling.

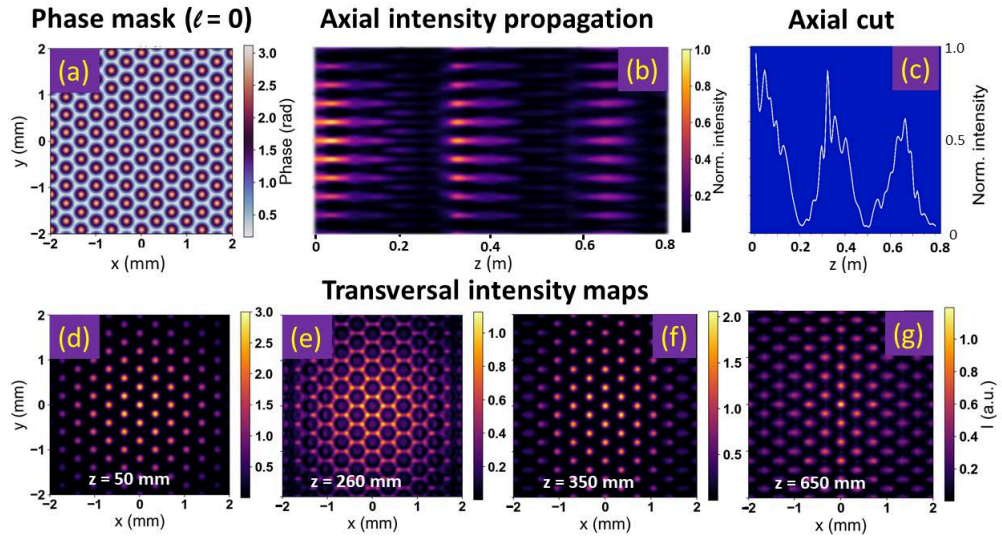


Figure 3. Spatial characteristics of the self-imaging of a NB-type STWP array (NB-A): (**a**) phase mask consisting of a hexagonal arrangement of identical axicons, (**b**) *y*-*z*-section in propagation direction z, (**c**) central linear cut in propagation direction crossing the focal plane and 2 subsequent nondiffracting Talbot peaks, (**d**) section cut through the focal plane, (**e**) out-of-phase section plane, (**f**) first nondiffracting Talbot plane, (**g**) second nondiffracting Talbot plane.

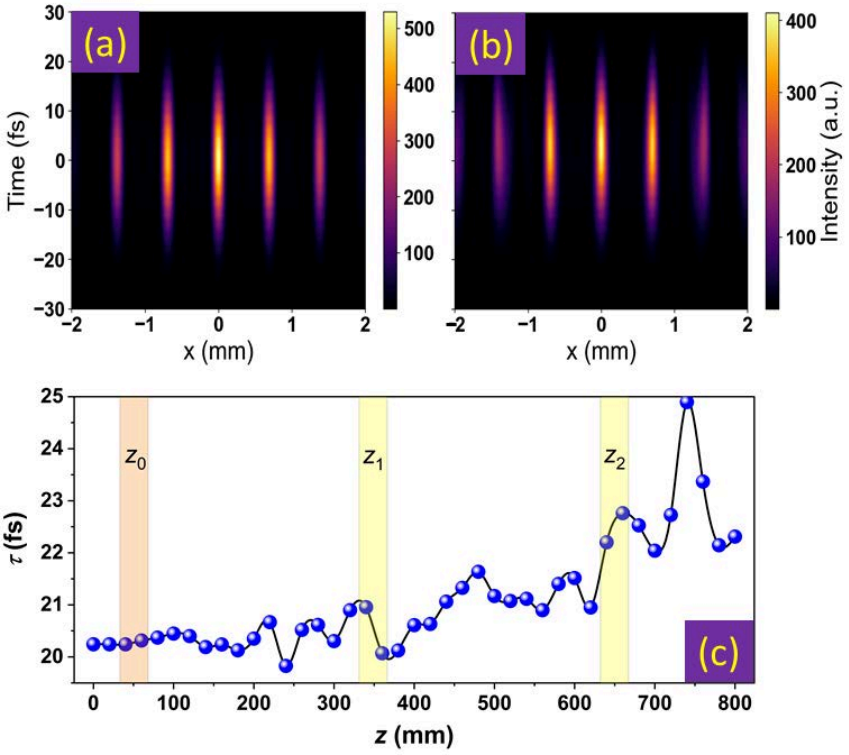


Figure 4. Temporal characteristics of a NB-type STWP array (NB-A) for an *x*-cut in two selected distances: (**a**) $z = 50$ mm, (**b**) $z = 350$ mm (first Talbot plane), (**c**) propagation-dependent temporal oscillation for the central position (z_0 = focal plane, z_1 = first Talbot plane, z_2 = second Talbot plane; parameters corresponding to Figure 3).

At an initial pulse duration of $\boldsymbol{\tau} = 20$ fs, the temporal structure of the pulse remains nearly unchanged in the first Talbot plane (theoretical deviation about $\Delta\boldsymbol{\tau} < 1$ fs) so that near field pulse information is transferred to a distant axial position and an array of BG-NBs is

available there for intensity-dependent applications as well. Within the second geometrical Talbot distance, the deviation from original pulse duration is <3 fs.

4.2.2. Propagation of Arrays of Nondiffracting Orbital Momentum Beams (OAM-A)

Further simulations were performed for a vortex-loaded NB array (OAM-A) with a topological charge of l = 1. Figure 5a shows a section of the beam-shaping phase map. The pulse transfer into nondiffracting self-images was studied by comparing the simulated time evolution closely behind the generating phase map and in the first geometrical Talbot plane (Figure 5b,c). All partial hollow beams at the first nondiffracting Talbot plane show a slight conical distortion (Figure 5c).

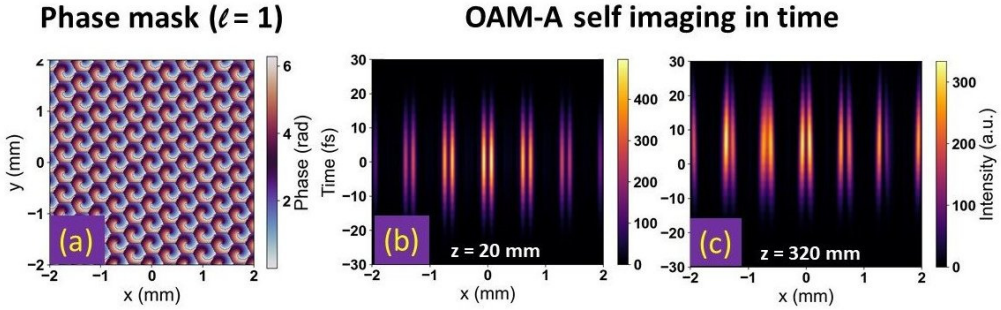


Figure 5. Temporal transfer of an array of vortex-type STWPs (OAM-A): (**a**) hexagonal arrangement of spiral phase plates, (**b**,**c**) *x*-*t* slices at axial distances $z = 20$ mm and $z = 320$ mm, respectively. The initial pulse duration is found to be nearly restored in the self-image of the STWP array within the first geometrical Talbot plane but a slight conical distortion in the sub-beams indicates specific spatio-temporal coupling effects.

5. Discussion

5.1. Bandwidth-Dependent Spectral Quality

With respect to the intensity propagation, the needle-like wavepackets according to *Method I* and *Method II* show rather marginal differences. We like to focus our discussion on the spectral aspects which often fall short or are completely neglected in the literature. To better visualize the difference in the spectral quality, the shift in the center wavelengths of both types of STWPs is compared by radial spectral profiles for a radial cut at the intensity maximum (Figure 6a). The bandwidth transfer for both approaches from the input to the axial intensity maximum is compared in Figure 6b.

In contrast to nondiffracting BG-NBs, which are generated by axicon-shaped phase elements (*Method I*), PS-GF-type STWPs are engineered via spatio-temporal and spatio-spectral coupling (*Method II*). The more complex design approach enforces a rigid, deterministic mapping between the transverse wave vector components and the wavelengths. Because of the finite input aperture, the geometric acceptance window for coupled wavelengths is strictly bounded. As the input spectral bandwidth increases beyond this critical threshold, the system acts as a spatial-frequency low-pass filter, resulting in spectral truncation. Consequently, the output bandwidth exhibits a distinct saturation behavior (red dashed line in Figure 6b), asymptotically approaching an absolute upper limit dictated by the maximum allowed cone-intersection span. This underscores a fundamental trade-off of PS-GF-type STWPs: while they achieve propagation invariance, their bandwidth and temporal compression limits are severely constrained by the finite aperture and angular acceptance of the optical system. The curves in Figure 6b indicate two different regimes. In the low-bandwidth regime, the output bandwidth of PS-GF-type STWPs exceeds the input value ($\Delta\lambda_{out} > \Delta\lambda_{in}$). This is a direct consequence of the spatial-frequency redistribution enforced

by spatio-temporal coupling, which maps transverse wave vectors to specific wavelengths, causing a localized spectral broadening. At larger input bandwidths, however, aperture-induced truncation and saturation dominate ($\Delta\lambda_{out} < \Delta\lambda_{in}$). Therefore, a comparison of both methods is not trivial and depends on the complete set of parameters.

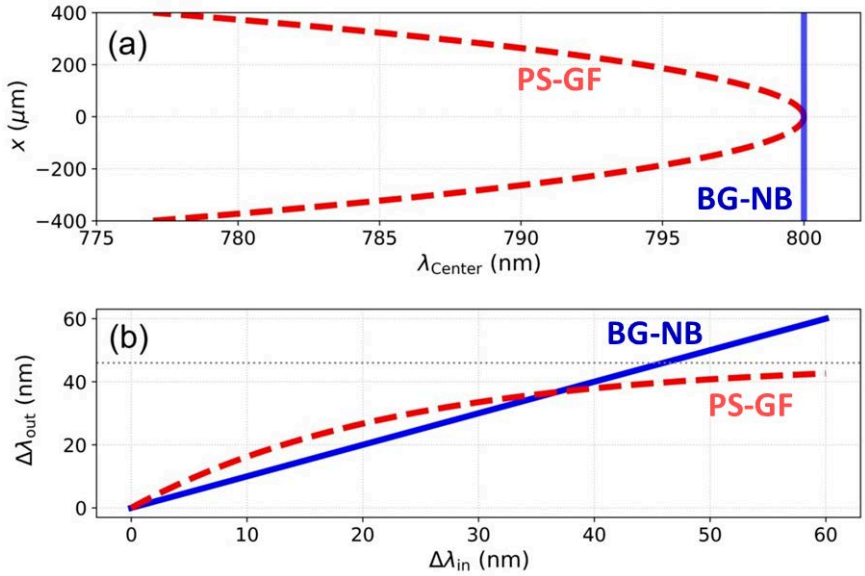


Figure 6. Comparison of BG-NB-type and PS-GF-type STWPs with respect to their spectral quality (data corresponding to Figure 2c,d): (**a**) The radial dependence of the central wavelengths in (**a**) shows a highly homogeneous spectrum along the radial coordinate for BG-NBs, whereas a significant shift appears for PS-GF; (**b**) The spectral transfer from the source (input bandwidth $\Delta\lambda_{in}$) to the axial centers of the wavepackets (output bandwidth $\Delta\lambda_{out}$) has linear characteristics for BG-NBs and saturation-like charateristics for PS-GF.

5.2. Nondiffracting Spatio-Temporal Self-Imaging of Arrays of STWPs

The simulations results for the arrangements convincingly confirm the findings four our earlier experiments involving SLM-generated arrays of NBs with varying topological charges [3,20]. The possibility to design self-imaging in space and time domains is a clear advantage for array-based and/or non-contact applications of ultrashort wavepackets and polychromatic beams. Under idealized conditions—free from diffraction and chirp—spatio-temporal coupling is caused by the phase differences between the partial beams of adjacent axicons. The temporal self-imaging (Figure 4) indicates that the temporal information of femtosecond laser pulses can be transferred from near-field to certain finite distances (geometrical Talbot planes). The geometrical dissipation leads to a limitation of the number of available Talbot planes. This could, in principle, be overcome in part by working with an outer reflector (light tunnel) redirecting the light in the interference zones. The local spatio-temporal contrast of the self-replicated wavepackets can serve as a criterion to quantitatively evaluate the self-imaging.

The self-images of the array of vortex beams (Figure 5c) show a slight conical distortion that is explained by a particular kind of spatio-temporal coupling. We assume that the deformation results from the interference of intertwined spectral compartments of vortex beams at large bandwidths. The sensitivity of this effect against the design parameters seems to be a rather complex problem and remains subject to further theoretical and experimental studies. Nonlinear and thermal effects were still not considered in our simulations but should be relevant for high-power applications and in wavelength regions with higher absorption of the liquid crystal pixels of an SLM.

To visualize the unique propagation properties of arrays of QND NBs, two Animations (S1 and S2) are provided as Supplementary Material.

6. Conclusions

To conclude, the propagation properties of different types of ultrafast STWPs were studied by numerical simulations. Special attention was paid to the concept of "highly localized wavepackets" [17–19] which considers more complex STWPs as compositions of "elementary" needle-shaped wavepackets. The decomposition into compact and easier-to-simulate elementary modes provides a practicable tool for designing and optimizing structured wavepackets and modeling their propagation.

A key motivation for investigating discretized approaches was the availability of high-resolution, low-dispersion liquid-crystal-on-silicon (LCoS) spatial light modulators (SLMs), which makes it possible to generate reconfigurable phase profiles and conduct corresponding experiments with pulse durations of only few cycles of the electric field in the near-infrared. Based on the example of a space–time vortex, it was demonstrated that decoupling the transverse beam geometry from the topological charge (or, in general, structured phase map) provides a robust framework for generating stable, arbitrarily sized, nondiffracting ultrafast optical fields.

In a first series of simulations, intensity propagation and spectral quality of femtosecond axicon-shaped needle beams (BG-NBs) were compared with spectrally pre-shaped Gaussian foci (PS-GF). Although resulting spatial intensity structures are very similar, a detailed analysis of the spectral quality indicates a higher radial spectral homogeneity of BG-NBs at short pulse durations for certain parameter windows. The relevance of the predicted wavelength gradients in the range of a few tenths of a nanometer - as predicted for pulses lasting only a few femtoseconds - depends significantly on the selectivity of specific applications, such as in resonant multiphoton absorption or excitation near the band gap. On the other hand, spectral signatures could be encoded purposefully in (PS-GF) for information transfer. Further improvements should be feasible by unifying the specific advantages of the different techniques of BG-NB and PS-GF to simultaneously shape phase and spectral profiles.

In a second series of simulations, array-specific propagation effects were analyzed for hexagonal arrangements of NBs and arrays of pulsed vortex beams. It was shown that the nondiffracting Talbot effect can even be observed at short pulse durations. The quality of self-imaging which, for example, can be defined by the number and contrast of detectable Talbot patterns, depends on spectral bandwidth and profile. The spatio-temporal coupling by travel time effects leads to a reduction in contrast and pulse duration during the propagation and has to be taken into account or compensated for practical applications. The transfer of pulse energy into intense and temporally ultrashort needle-like zones enables for new applications, e.g., in sensing and materials processing. The nondiffracting self-imaging phenomenon could be exploited to extract wavefront information by Shack–Hartmann sensors or for the highly parallel processing of surfaces or generating multiple plasma channels.

The results largely confirm previously published experimental results [3,20]. The slightly conical propagation of the partial STWPs within the Talbot planes of the OAM arrays are interpreted as an indication of a particular sort of spatio-temporal coupling by intertwined twisted spectral compartments. A more detailed analysis of this phenomenon is left for future research.

The key essential points are summarized as follows: Concerning the experimental realization, the generation of STWPs on the basis of QND NBs provides the ability to work at shorter pulse durations with less effort. A higher robustness and spectral quality can be reached by this approach. Higher intensities can be realized by the PS-GF. For the generation

of structured wavepackets, e.g., via the nondiffracting Talbot effect of arrays of STWPs, the NB approach is clearly advantageous.

7. Outlook

Currently, STWPs represent a fast developing topic with implications for fundamental theory as well as for technological applications. Our simulations for arrays were performed only for uniform arrangements consisting of identical elements. In general, however, more degrees of freedom can be explored by varying parameters. Recently, the case of aperiodic arrays (the Montgomery effect) was investigated by other authors [43]. Additional imaging properties may be obtained by nonuniform arrays with global envelope phase functions. The complementary relationship between QND STWPs and simultaneous spatio-temporal focusing [44] may stimulate further research on pulse front management, X-wave propagation [45,46] and rogue waves as manifestations of spectral interference in space and time. Design approaches based on space–time duality provide an appropriate frame for a generalized description [47]. Nanometer and attosecond STWPs [48] extend the length and time-scales to new limits. Recent success on STWP transfer in fibers may boost optical communication [49,50]. Accelerating wavepackets [51,52], metamaterials [53], structured vector wavepackets [54], optical skyrmions [55,56], frequency combs [57], and STWP-based analog computing [58] will contribute significantly to emerging quantum technologies. The specific degrees of freedom and the particular stability of OAM pulses are not only used in optical communication [59–61] but find many new fields of application, e.g., optical cell trapping [62] and the fabrication of nanophotonic structures [63,64]. Recently, femtosecond optical springs were formed by combining a hologram and an SLM [65]. To generate optical springs at relativistic intensities (up to 1.4×10^{18} W cm^{-2}) for structured laser–plasma interactions, off-axis spiral phase mirrors were used to manipulate helical phases of spectrally separated parts of broadband pulses and their coherent combinations [66]. Longitudinal management of STWPs [67] and the direct laser generation of wavepacket arrays [68] opens further prospects for advanced photonic solutions. The generation of perfect space–time vortices by focusing BG beams in space and time was theoretically suggested in the literature [69]. The capability of nanoprinted optical components for shaping needle beams of high aspect ratio was also recently demonstrated [70].

This list of current trends is not exhaustive. For a recently published comprehensive overview on the field of ultrafast optical vortices, we refer to ref. [71].

Supplementary Materials: The following supporting information can be downloaded at https://www.mdpi.com/article/10.3390/photonics13111088/s1, Video S1: Propagation of a 2D structured STWP consisting of an array of NBs; Video S2: Temporal evolution of a 2D structured STWP consisting of an array of NBs.

Author Contributions: Conceptualization and methodology, R.G. and M.B., software M.B.; data analysis, M.B. and R.G.; writing—original draft preparation, R.G.; writing—review and editing, R.G. and M.B.; visualization, M.B. and R.G.; project administration and funding acquisition, R.G.; All authors have read and agreed to the published version of the manuscript.

Funding: The studies on shaping of needle beams and STWPs were financially supported in parts by Deutsche Forschungsgemeinschaft (GR1782/16-1) and Laserlab-Europe (MBI 002528).

Data Availability Statement: No new experimental data were created or analyzed in this study. Data sharing is not applicable to this article.

Acknowledgments: Experimental resources including lab space and laser systems were kindly provided by Nathalie Picqué (MBI). The authors thank Jahns (FernUniversity, Hagen) for the stimulating discussions and Enda McGlynn (Dublin City University) for reviewing the text.

Conflicts of Interest: The authors declare no conflicts of interest.

References

1. Hernandez-Figueroa, H.E.; Zamboni-Rached, M.; Recami, E. (Eds.) *Non-Diffracting Waves*; John Wiley & Sons: Berlin, Germany, 2014.
2. Forbes, A. Structured light in space and time. *Photon. Insights* **2025**, *4*, C02-1−C02-2. [CrossRef]
3. Grunwald, R.; Bock, M. Needle beams: A review. *Adv. Phys. X* **2020**, *5*, 1736950. [CrossRef]
4. Berry, M.V.; Balazs, N.L. Nonspreading wave packets. *Am. J. Phys.* **1979**, *47*, 264–267. [CrossRef]
5. Malomed, B.A.; Mihalache, D.; Wise, F.; Torner, L. Spatiotemporal optical solitons. *J. Opt. B Quant. Semiclass. Opt.* **2005**, *7*, R53. [CrossRef]
6. Liu, X.; Cao, Q.; Zhan, Q. Spatiotemporal optical wavepackets: From concepts to applications. *Photonics Insights* **2024**, *3*, R08-1−R08-54. [CrossRef]
7. Kondakci, H.E.; Esat, H.; Abouraddy, A.F. Diffraction-free space–time light sheets. *Nat. Photonics* **2017**, *11*, 733–740. [CrossRef]
8. Yessenov, M.; Hall, L.A.; Schepler, K.L.; Abouraddy, A.F. Space-time wave packets. *Adv. Opt. Photonics* **2022**, *14*, 455–569. [CrossRef]
9. Abouraddy, A.F.; Yessenov, M.; Divliansky, I.; Watmik, A.T. New Frontiers in spatiotemporally structured light. *Opt. Photon. News* **2025**, *36*, 40–47. [CrossRef]
10. Durnin, J.; Miceli, J.J.; Eberly, J.H. Diffraction-free Beams. *Phys. Rev. Lett.* **1987**, *58*, 1499–1501. [CrossRef] [PubMed]
11. Grunwald, R.; Bock, M.; Kebbel, V.; Huferath, S.; Neumann, U.; Steinmeyer, G.; Stibenz, G.; Néron, J.-L.; Piché, M. Ultrashort-pulsed truncated polychromatic Bessel-Gauss beams. *Opt. Express* **2008**, *16*, 1077–1089. [CrossRef] [PubMed]
12. Durfee, G.; Gemmer, J.; Moloney, J.V. Phase-only shaping algorithm for Gaussian-apodized Bessel beams. *Opt. Express* **2013**, *21*, 15777–15786. [CrossRef] [PubMed]
13. Grunwald, R. *Thin-Film Microoptics—New Frontiers of Spatio-Temporal Beam Shaping*; Elsevier: Amsterdam, The Netherlands, 2007.
14. Hall, L.A.; Romer, M.A.; Turo, B.L.; Hayward, T.M.; Menon, R.; Abouraddy, A.F. Space-time wave packets propagating a kilometer in air. *J. Opt.* **2026**, *28*, 0956908. [CrossRef]
15. Grunwald, R.; Neumann, U.; Langer, S.; Stibenz, G.; Steinmeyer, G.; Kebbel, V.; Piché, M.; Néron, J.-L. Ultrabroadband spectral transfer in extended focal zones: Truncated few-cycle Bessel-Gauss beams. In *Conference on Lasers and Electro-Optics*; Paper CTuAA6; Optica Publishing Group: Washington, DC, USA, 2005.
16. Kurilkina, S.N.; Dovydenko, S.N. Formation and Propagation of needle light beams. *J. Appl. Spectrosc.* **2025**, *92*, 039–1044. [CrossRef]
17. Bock, M.; Das, S.K.; Grunwald, R. Ultrashort highly localized wavepackets. *Opt. Express* **2012**, *20*, 12563–12578. [CrossRef] [PubMed]
18. Grunwald, R.; Bock, M. Needle beams and structured space-time wavepackets. *arXiv* **2025**, arXiv:2512.03993.
19. Bock, M.; Das, S.K.; Grunwald, R. Adaptive generation and diagnostics of linear few-cycle light bullets. *Appl. Sci.* **2013**, *3*, 139–152. [CrossRef]
20. Bock, M.; Treffer, A.; Grunwald, R. Nondiffracting self-imaging of ultrashort wavepackets. *Opt. Lett.* **2017**, *42*, 2374–2377. [CrossRef] [PubMed]
21. Li, W.; Teng, H.; Liang, C.; Liu, J.; Cai, Y.; Liu, X. Spatiotemporal diffraction-free wave packets of the caustic waveforms. *Phys. Rev. A* **2026**, *113*, 033502. [CrossRef]
22. Saari, P. Spatially and temporally nondiffracting ultrashort pulses. In *Ultrafast Processes in Spectroscopy*; Svelto, O., De Silvestri, S., Denardo, G., Eds.; Plenum Press: New York, NY, USA, 1996; pp. 151–156.
23. Musigmann, M.; Jahns, J.; Bock, M.; Grunwald, R. Refractive-diffractive dispersion compensation for optical vortex beams with ultrashort pulse durations. *Appl. Opt.* **2014**, *53*, 7304–7311. [CrossRef] [PubMed]
24. Hall, L.A.; Yessenov, M.; Abouraddy, A.F. Space-time wave packets violate the universal relationship between angular dispersion and pulse-front tilt. *Opt. Lett.* **2021**, *46*, 1672–1675. [CrossRef] [PubMed]
25. Yessenov, M.; Hall, L.A.; Abouraddy, A.F. Engineering the optical vacuum: Arbitrary magnitude, sign, and order of dispersion in free space using space-time wave packets. *ACS Photonics* **2021**, *8*, 2274–2284. [CrossRef]
26. Hall, L.A.; Abouraddy, A.F. Non-differentiable angular dispersion as an optical resource. *J. Opt. Soc. Am. A* **2022**, *39*, 2016–2025. [CrossRef] [PubMed]
27. Hall, L.A.; Abouraddy, A.F. Canceling and inverting normal and anomalous group-velocity dispersion using space-time wave packets. *Laser Photonics Rev.* **2023**, *17*, 2200119. [CrossRef]
28. Hall, L.A.; Abouraddy, A.F. Spectral reorganization of space-time wave packets in presence of normal group-velocity dispersion. *Phys. Rev. A* **2025**, *111*, 063515. [CrossRef]

29. Kim, D.; Guo, C.; Catrysse, F.; Fan, S. Shaping space-time wave packets beyond the paraxial limit using a dispersion magnifier. *Phys. Rev. A* **2025**, *111*, 013504. [CrossRef]
30. Parker, K.J.; Alonso, M.A. The longitudinal iso-phase condition and needle pulses. *Opt. Express* **2014**, *24*, 28669.
31. Batavani, L.; Sabouri, S.G. Physics-inspired neural networks for tailored ripple-free optical needle beams. *Opt. Express* **2025**, *33*, 49189–49199. [CrossRef] [PubMed]
32. Wang, C.; Liang, Z.; Ruan, Z. Spatiotemporal optical wave packets with arbitrary trajectories. *Opt. Lett.* **2025**, *50*, 4114–4117. [CrossRef] [PubMed]
33. Bock, M.; Das, S.K.; Fischer, C.; Diehl, M.; Boerner, P.; Grunwald, R. Adaptive shaping of nondiffracting wavepackets for applications in ultrashort pulse diagnostics. In *Non-Diffracting Waves*; Hernandez-Figueroa, H.E., Zamboni-Rached, M., Recami, E., Eds.; John Wiley & Sons: Berlin, Germany, 2014; pp. 271–285.
34. Brunne, J.; Wapler, M.C.; Wallrabe, U. Fast and robust piezoelectric axicon mirror. *Opt. Lett.* **2014**, *39*, 4631–4634. [CrossRef] [PubMed]
35. Brunne, J.; Wallrabe, U. Tunable MEMS axicon mirror arrays. *Opt. Lett.* **2013**, *38*, 1939–1941. [CrossRef] [PubMed]
36. Bock, M.; Brunne, J.; Treffer, A.; König, S.; Wallrabe, U.; Grunwald, R. Adaptive spiral phase elements for the generation of few-cycle vortex pulses. In *Proceedings of the 2013 Conference on Lasers and Electro-Optics—International Quantum Electronics Conference*; Paper CFIE_11_3; Optica Publishing Group: Washington, DC, USA, 2013.
37. Gu, C.; Zhang, D.; Chang, Y.; Chen, S.-C. Digital micromirror device-based ultrafast pulse shaping for femtosecond laser. *Opt. Lett.* **2015**, *40*, 2870−2873. [CrossRef] [PubMed]
38. Grunwald, R.; Elsaesser, T.; Bock, M. Spatio-temporal coherence mapping of few-cycle vortex pulses. *Sci. Rep.* **2014**, *4*, 07148. [CrossRef] [PubMed]
39. Kondakci, H.E.; Abouraddy, A.F. Optical space-time wave packets having arbitrary group velocities in free space. *Nat. Commun.* **2019**, *10*, 929. [CrossRef] [PubMed]
40. Hall, L.A.; Yessenov, M.; Ponomarenko, S.A.; Abouraddy, A.F. The space–time Talbot effect. *APL Photonics* **2021**, *6*, 056105. [CrossRef]
41. Yessenov, M.; Free, J.; Chen, Z.; Johnson, E.G.; Lavery, M.P.J.; Alonso, M.A.; Abouraddy, A.F. Space-time wave packets localized in all dimensions. *Nat. Commun.* **2022**, *13*, 4573. [CrossRef] [PubMed]
42. Hall, L.A.; Ponomarenko, S.; Abouraddy, A.F. Temporal Talbot effect in free space. *Opt. Lett.* **2021**, *46*, 3107–3110. [CrossRef] [PubMed]
43. Yessenov, M.; Sacchi, L.; Palmieri, A.; Hall, L.A.; Abouraddy, A.F.; Capasso, F. Observation of spatially structured Montgomery effect in free space. *arXiv* **2025**, arXiv:2510.16269v1.
44. Kühn, D.; Treffer, A.; Wyrowski, F.; Grunwald, R. Simultaneous spatio-temporal focusing with pulse front symmetrization. *Opt. Lett.* **2022**, *47*, 750–753. [CrossRef] [PubMed]
45. Saari, P.; Reivelt, K. Evidence of X-Shaped Propagation-Invariant Localized Light Waves. *Phys. Rev. Lett.* **1997**, *79*, 4135–4138. [CrossRef]
46. Grunwald, R.; Kebbel, V.; Griebner, U. Generation and characterization of spatially and temporally localized few-cycle optical wavepackets. *Phys. Rev. A* **2003**, *67*, 063820. [CrossRef]
47. Chen, W.; Yu, A.Z.; Zhou, Z.; Ma, L.-L.; Wang, Z.-Y.; Yang, J.C.; Qiu, C.-W.; Lu, Y.-Q. Tailoring spatiotemporal wavepackets via two-dimensional space-time duality. *Nat. Commun.* **2025**, *16*, 2818. [CrossRef] [PubMed]
48. Porras, M.A. Optics of spatiotemporal optical vortices for atto-and nano-photonics. *Nanophotonics* **2025**, *14*, 845–852. [CrossRef] [PubMed]
49. Su, X.; Zou, K.; Wang, Y.; Yessenov, M.; Zhou, H.; Song, H.; Ko, W.; Zeng, R.; Alhaddad, A.; Ramakrishnan, M.; et al. Space-time wave packets in multimode optical fibers with controlled dynamic motions and tunable group velocities. *Nat. Commun.* **2025**, *16*, 2027. [CrossRef] [PubMed]
50. Su, X.; Wang, Y.; Willner, A.E. Photonics Breakthroughs 2025: Space-time Wave Packets in Fibers. *IEEE Photonics J.* **2026**, *18*, 3300106. [CrossRef]
51. Wang, H.; Chen, W.; Li, D.; Xue, J.; Sun, Y.; Zhang, H.; Zeng, C.; Wie, B.; Mao, D. Generation of self-healing spatiotemporal Airy wavepackets based on discrete frequency and geometric phase modulation. *Chin. Opt. Lett.* **2025**, *23*, 091405. [CrossRef]
52. Hall, L.A.; Abouraddy, A.F. Bending space-time wave packets. *Opt. Lett.* **2025**, *50*, 5829–5832. [CrossRef] [PubMed]
53. Engheta, N. Metamaterials with high degrees of freedom: Space, time, and more. *Nanophotonics* **2021**, *10*, 639–642. [CrossRef]
54. Yessenov, M.; Chen, Z.; Lavery, M.P.J.; Abouraddy, A.F. Vector space-time wave packets. *Opt. Lett.* **2022**, *47*, 4131–4134. [CrossRef]
55. Teng, H.; Liu, X.; Zhang, N.; Fan, H.; Chen, G.; Cao, Q.; Zhong, J.; Lei, X.; Zhan, Q. Construction of optical spatiotemporal skyrmions. *Light Sci. Appl.* **2025**, *14*, 324. [CrossRef] [PubMed]
56. Zhang, Y.; Zhou, Z.; Zhang, S.; Zhang, Y.; Min, C.; Yuan, X. Spatiotemporal Hermite-Gaussian skyrmions. *Opt. Lett.* **2026**, *51*, 6086–6089. [CrossRef] [PubMed]

57. Willner, A.E.; Su, X.; Zuo, Y.; Wang, Y.; Jiang, Z.; Minoofar, A.; Lian, H.; Zhao, Z.; Alhaddad, A.; Zheng, R. Synthesis of space-time wave packets using correlated frequency comb and spatial field. *Nanophotonics* **2025**, *14*, 659–675. [CrossRef] [PubMed]
58. Huang, J.; Zhao, D.; Shi, J.; Zhang, H.; Wang, H.; Sun, F.-W.; Zhan, Q.; Zhu, S.; Huang, K.; Ruan, Z. Experimental demonstration of spatiotemporal analog computation in ultrafast optics. *Light Sci. Appl.* **2026**, *15*, 77. [CrossRef] [PubMed]
59. Willner, A.E.; Huang, H.; Yan, Y.; Ren, Y.; Ahmed, N.; Xie, G.; Bao, C.; Li, L.; Cao, Y.; Zhao, Z.; et al. Optical communications using orbital angular momentum beams. *Adv. Opt. Photon.* **2015**, *7*, 66–106. [CrossRef]
60. Obaid, O.; Malhi, K.S.; Kaur, M. A Comprehensive Review of OAM-Based Free-Space Optical Communication System Design, Atmospheric Challenges and Emerging Techniques. *Int. J. Comp. Inform. Syst. Ind. Manag. Appl.* **2026**, *18*, 1075–1085. [CrossRef]
61. Gong, L.; Zhao, Q.; Zhang, H.; Hu, X.-Y.; Huang, K.; Yang, J.-M.; Li, Y.-M. Optical orbital-angular-momentum-multiplexed data transmission under high scattering. *Light Sci. Appl.* **2026**, *8*, 27.
62. Qiao, Z.; Xie, G. Ultrafast and ultra-intense optical vortices: Advances, applications, challenges, and perspectives. *Appl. Phys. Rev.* **2026**, *13*, 041323-1–041323-32. [CrossRef]
63. Liu, J.; Yao, T.; Guo, Z.; Hu, M.; Zeng, H. Direct Generation of Tunable Femtosecond Vortex Arrays in a Yb:CALGO Laser. *Laser Photon Rev.* **2026**, e72143. [CrossRef]
64. Ponomarenko, S.A.; Hebri, D. Perfect space-time vortices. *Opt. Lett.* **2024**, *49*, 4322–4325. [CrossRef] [PubMed]
65. Li, R.; Zhang, Y.; Xin, W.; Sun, Y.; Sun, W.; Meng, C.; Guo, Y.; Zhang, X.; Lamon, S.; Yu, H. Two-photon-nanoprinted Pancharatnam–Berry phase element for compact high-aspect-ratio optical needle generation. *Opt. Express* **2026**, *34*, 43361–433670. [CrossRef]
66. Yang, L.; Ji, S.; Xie, K.; Du, W.; Liu, B.; Hu, Y.; Li, J.; Zhao, G.; Wu, D.; Huang, W.; et al. High efficiency fabrication of complex microtube arrays by scanning focused femtosecond laser Bessel beam for trapping/releasing biological cells. *Opt. Express* **2017**, *25*, 8144–8157. [CrossRef] [PubMed]
67. Yang, L.; Qian, D.S.; Xin, C.; Hu, Z.; Ji, S.; Wu, D.; Hu, Y.; Li, J.; Huang, W.; Chu, J. Direct laser writing of complex microtubes using femtosecond vortex beams. *Appl. Phys. Lett.* **2017**, *110*, 221103. [CrossRef]
68. Ni, J.; Huang, C.; Zhou, L.-M.; Gu, M.; Song, Q.; Kivshar, Y.; Qiu, C.-W. Multidimensional phase singularities in nanophotonics. *Science* **2021**, *374*, eabj0039. [CrossRef] [PubMed]
69. Franco, E.; Martínez-Matos, Ó.; Rodrigo, J.A. Flying spring and multi-ring ultrashort laser pulses with tunable wavefield dynamics. *Photon. Res.* **2025**, *13*, 1872–1886. [CrossRef]
70. Longman, A.; Attiyah, D.; Grace, E.S.; Gardner, C.; Suratwala, T.; Tham, G.; Harthcock, C.; Fedosejevs, R.; Dollar, F. Spatiotemporal shaping of broadband helical light pulses at relativistic intensities. *Nat. Photon.* **2026**, 843–849.
71. Su, X.; Zou, K.; Zhou, H.; Song, H.; Wang, Y.; Zeng, R.; Jiang, Z.; Duan, Y.; Karpov, M.; Kippenberg, T.J.; et al. Temporally and longitudinally tailored dynamic space-time wave packets. *Opt. Express* **2024**, *32*, 26653–26666. [CrossRef] [PubMed]

Disclaimer/Publisher's Note: The statements, opinions and data contained in all publications are solely those of the individual author(s) and contributor(s) and not of MDPI and/or the editor(s). MDPI and/or the editor(s) disclaim responsibility for any injury to people or property resulting from any ideas, methods, instructions or products referred to in the content.